

Determination of Brillouin backscattering strain and temperature coefficients in telecommunication optical fibers

Mateusz Łakomski, Bartłomiej Guzowski, Mateusz Plona, and Krzysztof Pęczek

Abstract—In this paper, the Brillouin spectra of silica-based optical fibers were investigated, and their temperature and strain dependence were determined. The values of the thermal coefficients are more diverse than those of the strain, based on the twelve commercially available optical fibers. The values ranging from 1.1 to 1.4 MHz/°C and from 0.043 to 0.053 MHz/με for the thermal and strain coefficients, respectively. Furthermore, the temperature influence on Brillouin frequency shift was measured for tight buffer and loose tube type cables. Long-term measurements of the outside ambient temperature were carried out to determine the absolute error in comparison to thermocouple.

Keywords—Brillouin scattering; distributed sensor; optical fiber; temperature

I. INTRODUCTION

OPTICAL fiber sensing technology has matured into a versatile and powerful tool for monitoring and visualizing in real-world applications through its unique sensing capabilities and compatibility with communication networks. Such a technology that works with telecommunication optical fibers is Brillouin backscattering. The main advantages are high sensitivity and the possibility of distributed sensing of strain and temperature along the length of the fiber over several to tens of kilometers with satisfying resolution [1-3], which makes them unrivaled over their electrical sensor counterparts. These sensing capabilities enable a wide range of applications in fields like structural health monitoring [4-5], submarine and pipeline sensing [6-7], security [8], and more. The principle of operation is based on the interaction of the photons of incident light with acoustic phonons traveling along the optical fiber. Due to this, a small portion of incident light is backscattered, whereas its frequency undergoes an upshift or downshift. The Brillouin frequency shift is expressed as follows [9]:

$$v_{SBS} = 2 \frac{n_{eff} v_A}{\lambda} \quad (1)$$

where: v_{SBS} – Brillouin frequency shift, n_{eff} – effective refractive index of optical fiber, v_A – speed of the acoustic wave in the optical fiber, λ_L – wavelength of laser source.

Fig. 1 shows some examples of Brillouin characteristics for

Authors are with Lodz University of Technology, Department of Semiconductor and Optoelectronic Devices, Łódź, Poland (e-mail: mateusz.lakomski@p.lodz.pl, ORCID: <https://orcid.org/0000-0002-1341-0215>,

different types of silica-based optical fibers. This variety is based on the ITU-T (International Telecommunication Union Telecommunications Standardization Sector) telecommunications standard dedicated to fiber optics. The difference in characteristics occurs not only between different ITU-T demands, but also within the same standard and, moreover, even comes from the same manufacturer. Detailed results and analyses are presented in the previous work [10]. For sensing applications, the desired type is a narrow spectrum with high intensity. It is well known that the Brillouin backscattering phenomenon depends mainly on the optical properties and geometry of the fiber [11-12]. In the first case, the refractive index and its distribution, transmitted wavelength, and mode confinement [13] of the optical signal impact the Brillouin scattering. On the other side, the size and shape of the optical fiber, such as the core diameter and its number [14-15], can influence the acoustic wave propagation also.

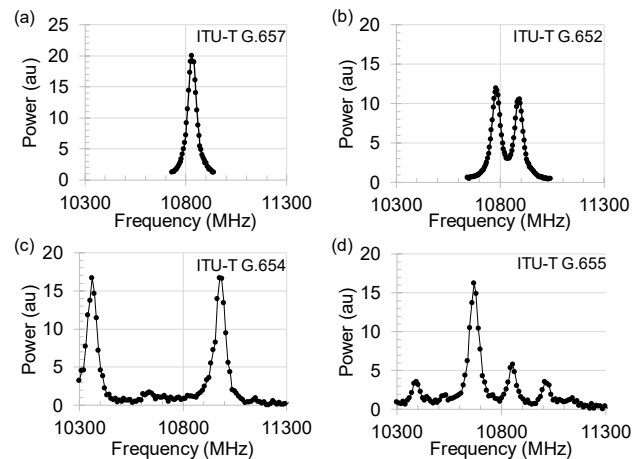


Fig. 1. Brillouin spectra of various telecommunication optical fibers according to ITU-T: G.657 (a), G.652 (b), G.654 (c), G.655 (d)

Additionally, the Brillouin backscattering effect is a non-linear in terms of the laser source parameters: intensity [16], pulse width [17], or coherence of the incident laser light. All of them can affect on the transition from spontaneous to stimulated Brillouin scattering and influence the efficiency of the sensing system [9]. Due to this, the shape of the characteristics and the number of observed peaks in the entire spectrum can vary [10,

<https://orcid.org/0000-0002-6090-1359>, <https://orcid.org/0009-0007-4745-0278>, <https://orcid.org/0009-0009-4566-9123>).



17]. Regardless, each peak typically drifts in response to changes in the longitudinal strain or temperature along the fiber. The induced shift of the frequency is linear, which is the basis for distributed Brillouin sensing:

$$v_{\text{SBS}} = v_{\text{B0}} + C_T(T - T_0) + C_\varepsilon(\varepsilon - \varepsilon_0) \quad (2)$$

where: v_{B0} - initial Brillouin frequency, C_T , C_ε - thermal and strain coefficients of optical fiber, T , ε - measured temperature and strain value, T_0 , ε_0 - reference temperature and strain value.

Brillouin backscattering in optical fibers is influenced by the acoustic, optical, geometric, environmental, and laser properties of the system, including active devices, as well as the optical fiber itself. Understanding and controlling these factors is crucial for optimizing Brillouin-based detection and other applications. In this paper, characterization using the BOTDR system of 12 commercially available optical fibers was done to show the differences in thermal and strain coefficients, which have to be taken into account e.g. in sensor application in coexistence with the FTTX network (Fiber To The X).

II. MATERIALS AND METHOD

In Table 1, the used samples of optical fibers are listed with their parameters for the 1550 nm wavelength: effective group index of refraction n_{eff} , mode field diameter MFD, and attenuation. As can be noticed, the samples represent different types of ITU-T standards and in some cases, various manufacturers.

The setup for temperature and strain coefficient measurement is shown in Fig. 2. The optical system is based on a Brillouin Optical Time Domain Reflectometer (BOTDR) unit from OZOptics. During the measurements, the minimal spatial resolution and spatial step were equal to 1 m (pulse width of 10 ns) and 0.5 m, respectively. The BOTDR was based on 1550 nm wavelength laser and was connected to the fiber under test through a 50 m long optical fiber jumper with an angled physical connector to minimize signal loss due to reflections.

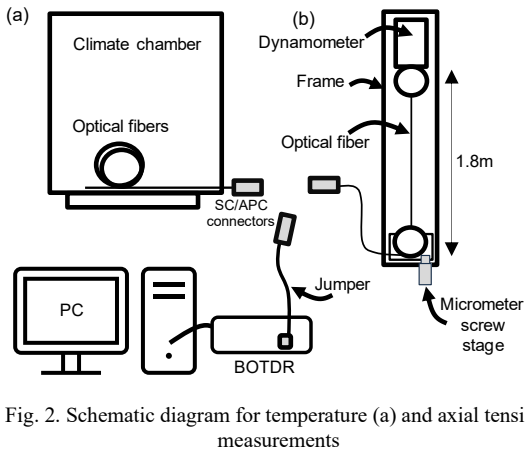


Fig. 2. Schematic diagram for temperature (a) and axial tensile (b) measurements

For the purpose of temperature cycle measurements, the optical fibers were connected in series using fusion splices and then placed into the dynamic climate chamber Binder MKT115. The optical path baseline at room temperature is shown in Fig. 3. As can be noticed, the fibers were sorted due to their main Brillouin frequency spectrum, and the total length was equal to about 0.7 km. Clearly visible peaks on the graph indicate the

TABLE I
TECHNICAL DATA OF TESTED OPTICAL FIBERS FOR 1550 NM WAVELENGTH

No.	ITU-T	n_{eff} (-)	MFD ^a (μm)	Attenuation (dB/km)
#1	G.652.D	1.4679	10.4±0.5	≤0.20
#2	G.652.D	1.4682	10.4±0.5	≤0.20
#3	G.654.C	1.462	10.5±0.5	≤0.16
#4	G.654.E	1.4650	12.4±0.5	≤0.17
#5	G.655.C	1.4700	8.4±0.6	≤0.22
#6	G.655.D	1.4693	9.6±0.4	≤0.19
#7	G.657.A1	1.467	10.3±0.5	≤0.18
#8	G.657.A1	1.468	9.9±0.5	≤0.21
#9	G.657.A2	1.4677	9.6±0.5	≤0.20
#10	G.657.A2	n.a.	10.4±0.5	≤0.20
#11	G.657.B3	1.4677	9.65±0.5	≤0.20
#12	G.657.B3	1.468	9.8±0.6	≤0.21

locations of splices between different types of optical fibers. Due to the disturbance in the homogeneous structure of the optical fiber core, random Brillouin frequency readings occur in these regions. During temperature tests, the chamber value was ranging from -20°C to $+70^\circ\text{C}$. To exclude the influence of Brillouin optical signal strength, the measurements were repeated 3 times and compared for both ends of the optical path.

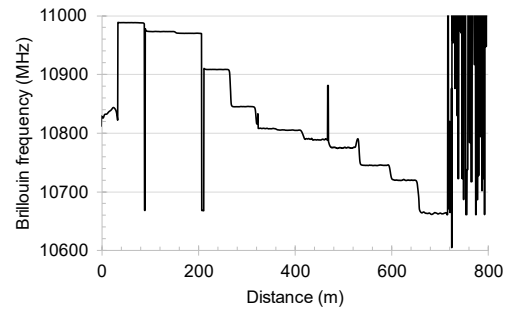


Fig. 3. Baseline of optical path including twelve bare optical fibers

To induce linear deformation of the optical fiber, the frame schematically presented in Fig. 2b was used. The 1.8 m long fiber under test was placed in the holder of the dynamometer from one side and in the micrometer positioning stage on the other. The maximum available tensile test was carried out for standard silica-based optical fiber, and the result is presented in Fig. 4. The linear response was observed for tensile deformation of optical fiber up to $7777 \mu\text{e}$, which corresponds to 14 mm elongation of 1.8 m long optical fiber. During further research using various optical fiber samples, tests were repeated 3 times for tensile and compressive strain measurements.

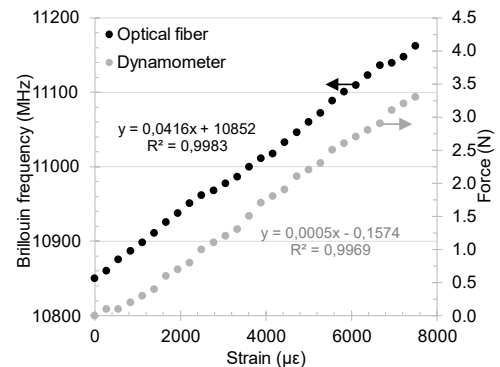


Fig. 4. Brillouin frequency shift of standard silica-based optical fiber during tensile test

The second part of research was concentrated on temperature measurement of different type of optical fiber construction, as a valuable supplement to tests of bare optical fiber. The construction of optical fiber cables is dependent on environmental conditions and installation requirements, with outdoor and underwater cables typically featuring more complex, layered protection than indoor ones.

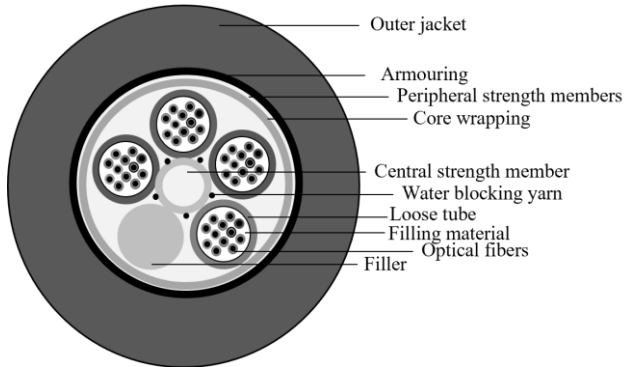


Fig. 5. Example optical fiber cable construction for outside applications

Fig. 5 presents a cross section of an example cable. A central, internal strength member, typically composed of fiberglass or a composite material, serves to absorb mechanical stress during the use, thereby protecting the optical fiber tubes. The role of buffer coatings for tubes, which can be divided into loose or tight buffers, is also significant. Loose tube permit the single or multiple number of optical fibers to move within the sheath, thereby reducing stress transmission. Conversely, tight tube construction provide high crush resistance, although this may result in increased stress under high loads. The incorporation of aramid yarns, enhances the tensile strength of the cable, absorbing tensile forces and preventing stress transfer to the optical fiber. The outer jacket, composed of materials such as PE (polyethylene) or PVC (polyvinyl chloride), serves to safeguard against mechanical damage and environmental factors. Moreover, flexible jackets are designed to absorb vibrations, while rigid ones offers higher crush resistance. Furthermore, some cables utilize protective gel or fillers that stabilize the fiber and cushion it against shocks and vibrations.

Taking all these variables into account, the proper design of a fiber optic cable is important to minimize impact of external factors on measurements and can affect on the performance and durability of the cable. Simultaneously, the possibly internal stresses coming from cable construction on Brillouin frequency shift have to be consider to avoid temperature reading mistakes.

III. RESULTS

A. Strain coefficient

As a result of the impact of the tensile force on the optical fiber, the Brillouin frequency drifts towards a higher frequency. Simultaneously, the signal level is slightly decreasing. The example spectrum shift is shown in Fig. 6, where experimental data were fitted by the Lorentzian function.

In Fig. 7, the comparison of strain coefficient results for different optical fibers is presented. The results ranging from 0.043 MHz/ $\mu\epsilon$ to 0.053 MHz/ $\mu\epsilon$ for all tested optical fibers. In our opinion, there is no significant difference in measured strain coefficients, and it is difficult to distinguish outstanding optical

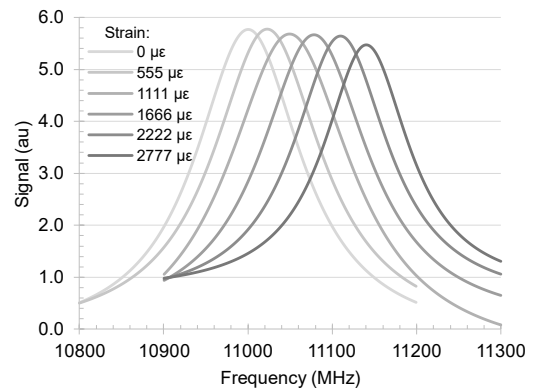


Fig. 6. Influence of tensile force on optical fiber Brillouin spectrum

fiber types for strain sensor applications. The sensitivity may be strongly dependent on the manufacturer’s production technique itself, as proven by the results for both G.652.D optical fibers.

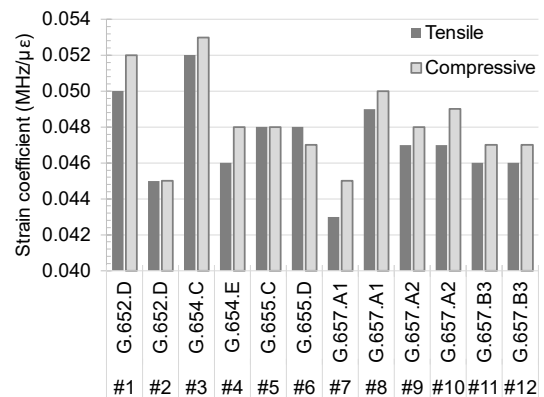


Fig. 7. Comparison of strain coefficient results for different optical fibers

B. Thermal coefficient

In the case of temperature measurements, the Brillouin frequency shift towards a higher frequency is observed when the temperature increases (Fig. 8). Nevertheless, in contrast to the strain measurements, the signal level is increasing. Fig. 9 summarizes the thermal coefficient values for twelve optical fibers, distinguishing the results achieved for heating and cooling cycles. The ITU-T G.654 type of optical fibers reaches higher values of thermal coefficient than the other types. Moreover, the differences in results among the same type but various manufacturers are also observed (e.g. G.657.A1).

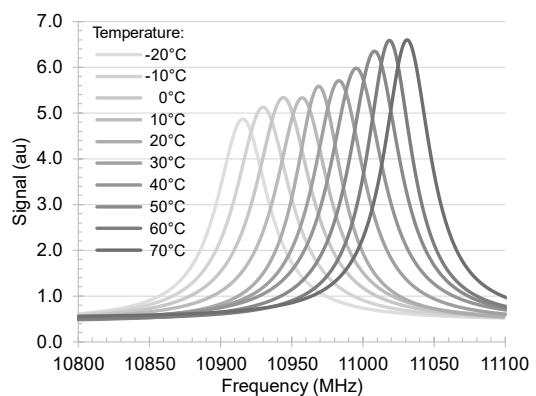


Fig. 8. Influence of temperature on optical fiber (#4) Brillouin spectrum

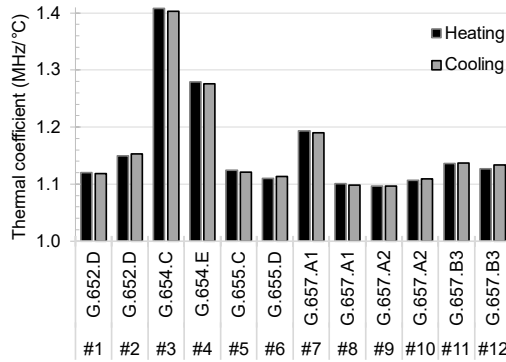


Fig. 9. Comparison of thermal coefficient results for different optical fibers

The aim of this research on bare optical fibers was to find the correlation between the achieved coefficients and their optical parameters. No significant correlation was observed between the strain coefficient and the variables. However, in Fig. 10, the observation for the thermal coefficient is present. Based on datasheet information (Tab. 1), it can be noticed that as the refractive index of optical fiber increases, the value of the measured coefficient decreases. A similar situation applies to the maximum attenuation of the optical fiber, however, stabilizes above the value of 0.19 dB/km.

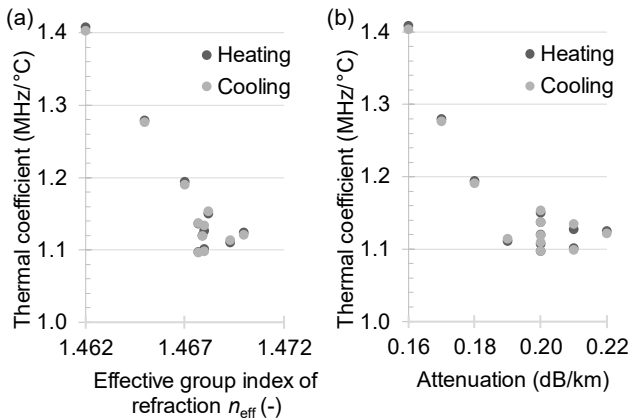


Fig. 10. Influence of effective group index of refraction (a) and attenuation of optical fiber (b) on the thermal coefficient.

C. Optical cable construction

The presented above results shows variety of determined coefficients. Nevertheless, the obtained characteristics in their temperature range were characterized by the high linearity. Next, the measurement of thermal coefficient of optical fibers in four different cable construction, shown in Fig. 11, were done. Loose-tube cable including 12 optical fibers and gel filled allows for their movement, thereby protecting it from mechanical stress. In contrast, tight-buffer designs hold the fiber more securely, offering crush protection but potentially exposing it to tensile stress. For both cables the outer sheath was made from PU (polyurethane) with 0.7 mm and 0.3 mm thickness, respectively for loose tube and tight buffer type cable.

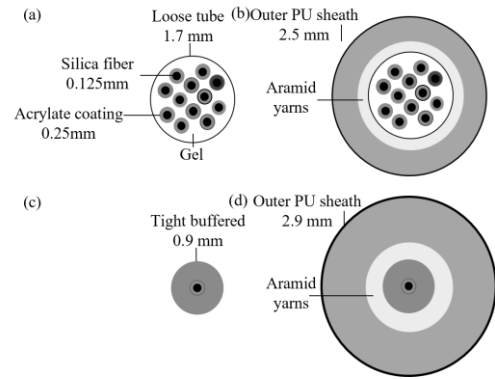


Fig. 11. Optical fiber cables construction cross sections: 12-fiber loose tube without (a) and with outer sheath (b), single fiber tight buffer without (c) and with outer sheath (d).

To determine their Brillouin frequency shift the temperature were ranging from -10°C to $+70^{\circ}\text{C}$, with 10°C step, and repeated as one cycle including heating and cooling processes. Before test, the thermal time constants for cables were determined and taken into account. In Fig. 12 the baseline of tested optical fiber link is presented. The Brillouin frequency results for these cables may indicates on initial stresses, and their value fluctuates depending on the type of cabling. It is particularly evident in the case of a tight buffer cable, where the frequency is about 50 MHz higher for the cable without outer PU jacket.

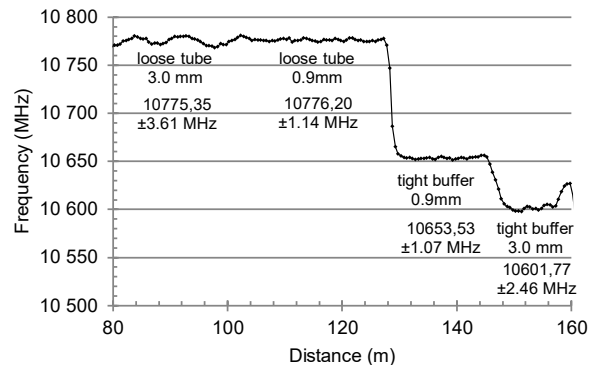


Fig. 12. Baseline of optical path for optical fiber cabling test.

Fig. 13 present dependence of temperature on the Brillouin frequency shift for all tested cables. The thermal shift obtained for the both loose tube cable samples exhibit a high degree of linearity. The small difference in readings is only visible around 0°C . The achieved thermal coefficient is slightly lower for the loose tube without additional outer PU sheath. In the second case, the determination of reliable and repeatable value of thermal coefficient is more challenging. The evident hysteresis is present for both samples of tight buffer cables. The both characteristics have rather polynomial tendency than linear. Only for tight buffer cable in 0.9 mm outer jacket a linear relationship is noticeable in a limited range from 30 to 70°C . Nevertheless, further research is required to confirm the repeatability of this finding.

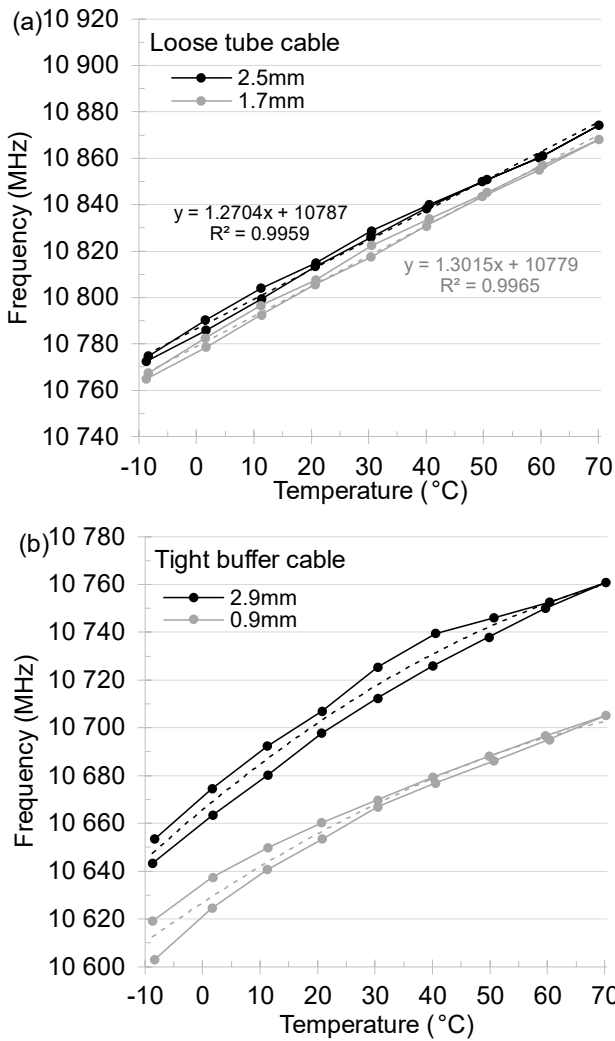


Fig. 13. Influence of temperature on Brillouin frequency shift for loose (a) and tight buffer (b) cables.

D. Long-term application test

Long-term measurement of ambient temperature in outdoor conditions were carried out using: a single, bare optical fiber (covered with a 245 μm acrylic coating) and loose-tube cable construction (with outside jacket with 2.5 mm diameter) with a total length of approximately 50 m. The measurements were taken occasionally during a period of 5 month, including the summer, autumn, and winter seasons. During this period of time, the ambient temperature was also read from the K-type thermocouple.

Fig. 14 and Fig. 15 presents the achieved results for both optical fibers. The temperature value for optical method of measurement was calculated using Eg. (2) using the previously determined values of the thermal coefficients. As the samples was loosely placed and loose tube cable was used, it was assumed that strain component was not occurred during measurement. The absolute error (related to secondary axis) is defined here as the difference between readings from the optical fiber and thermocouple. As can be noticed for the bare optical fiber results, the absolute error of temperature is significant. Importantly, the hot or cold season does not affect on that error level. The use of optical fiber cable with additional covering significantly improves these outcomes, as can be seen in Fig. 15.

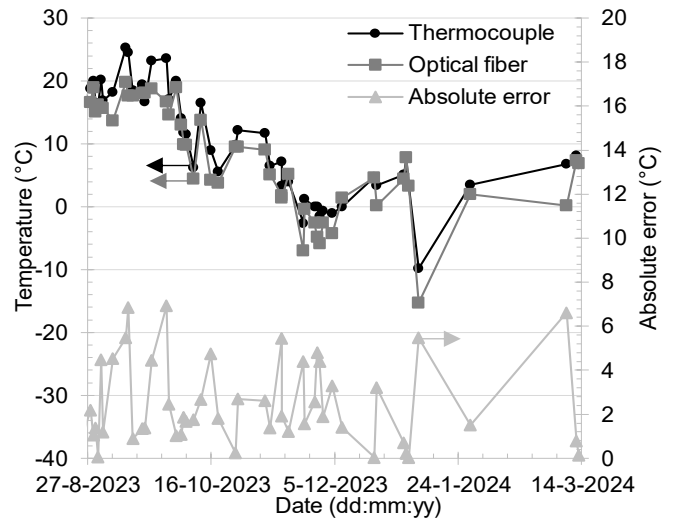


Fig. 14. Long-term measurement of ambient temperature using bare optical fiber.

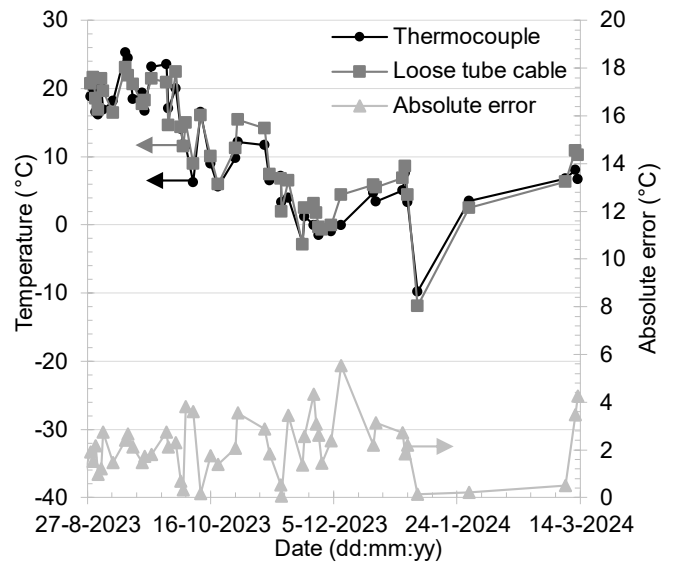


Fig. 15. Long-term measurement of ambient temperature using optical fiber in loose tube type cable.

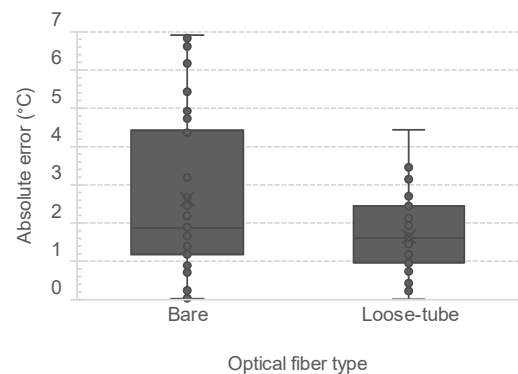


Fig. 16. Absolute error comparison for both tested optical fiber types.

However, the accuracy of readings using optical fiber and the BOTDR device is worth attention. On the one hand, the accuracy of the BOTDR device's temperature measurement is 0.8°C only. On the other hand, many external factors may

influence on the fluctuation of Brillouin frequency. The graph in Fig. 16 shows the comparison between values of the absolute errors for both optical fibers from whole measurement (N=52). The average value is 59% higher for the use of bare optical fiber. The maximum error at the level of about 7°C is unacceptable for this application. Besides the fact that both optical fibers were loosely placed, the most significant impact on temperature readings could be the changes in humidity or solar radiation. Due to this fact, the use of bare fiber is not recommended for application in an outside environment without any additional cable coatings.

IV. CONCLUSIONS

Among the tested samples, the highest thermal and strain coefficients were obtained for the ITU-T G.654.C compatible optical fiber type. One can notice that fiber has the lowest effective group index of refraction n_{eff} and attenuation, whereas relatively high value of mode field diameter. Based on the datasheet information, it was generally observed that the decrease of n_{eff} influences the increase in the value of the thermal coefficient. For the strain coefficient, no significant correlation was noted. However, the internal stresses have to be taken into account when optical fiber with additional outer jackets is using. The long-term measurements of outside ambient temperature using bare optical fiber confirmed a significant influence of external factors on the temperature readings. The absolute error was definitely lower for the results achieved using optical fiber in loose-tube cable.

REFERENCES

- [1] H. Wu et al., "High-performance distributed dynamic strain sensing by synthesizing ϕ -OTDR and BOTDR," *Opt. Express*, Vol. 31, Iss. 11, pp. 18098-18108, 2023. <https://doi.org/10.1364/OE.484529>
- [2] X. Liu, X. Bao, "Brillouin spectrum in LEAF and simultaneous temperature and strain measurement," *J. Light. Technology*, Vol. 30, Iss. 8, pp. 1053-1059, 2012. <https://doi.org/10.1109/JLT.2011.2168193>
- [3] H. Wu et al., "Enhancing spatial resolution of BOTDR sensors using image deconvolution," *Opt. Express*, Vol. 30, Iss. 11, pp. 19652-19664, 2022. <https://doi.org/10.1364/OE.459519>
- [4] A. M. Biondi et al., "Smart textile embedded with distributed fiber optic sensors for railway bridge long term monitoring," *Opt. Fiber Technol.*, Vol. 80, no. 103382, 2023. <https://doi.org/10.1016/j.yofte.2023.103382>
- [5] M. Lakomski, G. Tosik, P. Niedzielski, "Optical Fiber Sensor for PVC Sheet Piles Monitoring," *Electronics*, Vol. 10, Iss. 10, no. 1604, 2021. <https://doi.org/10.3390/electronics10131604>
- [6] F. Wang et al., "Research on the leakage monitoring of oil pipeline using BOTDR," *2016 Progress in Electromagnetic Research Symposium (PIERS)*, Shanghai, China, pp. 4907-4910, 2016. <https://doi.org/10.1109/PIERS.2016.7735790>
- [7] L. Zhao et al., "On-line monitoring system of 110 kV submarine cable based on BOTDR," *Sens. Actuators A: Phys.*, Vol. 216, pp. 28-35, 2014. <https://doi.org/10.1016/j.sna.2014.04.045>
- [8] X. Zheng et al., "Security pre-warning system of underground pipelines based on BOTDR," *Proc. SPIE 11607*, Optics Frontiers Online 2020: Distributed Optical Fiber Sensing Technology and Applications, No. 116070K, 2021. <https://doi.org/10.1117/12.2585489>
- [9] F. Mitschke, "Fiber Optics Physics and Technology," *Springer Berlin, Heidelberg*, pp. 182-188, 2009. <https://doi.org/10.1007/978-3-642-03703-0>
- [10] [10] Lakomski M., Tosik, G., Brillouin backscattering analysis in recent generation of telecom optical fibers, *Opt. Appl.*, Vol. 52 (2022), No. 3, pp. 405-416, 2004. <https://doi.org/10.37190/oa220307>
- [11] L. Zou et al., "Dependence of the Brillouin frequency shift on strain and temperature in a photonic crystal fiber," *Opt. Lett.*, Vol. 29, Iss. 13, pp. 1485-1487, 2004. <https://doi.org/10.1364/OL.29.001485>
- [12] W. Zou et al., "Investigation of Strain- and Temperature-Dependences of Brillouin Frequency Shifts in GeO₂-Doped Optical Fibers," *J. Light. Technology*, Vol. 26, Iss. 13, pp.1854-1861, 2008. <https://doi.org/10.1109/JLT.2007.912052>
- [13] P. D. Dragic et al., "Single- and few-moded lithium aluminosilicate optical fiber for athermal Brillouin strain sensing," *Opt. Lett.*, Vol. 40, Iss. 21, pp. 5030-5033, 2015. <https://doi.org/10.1364/OL.40.005030>
- [14] Y. Li et al., "Bend-tolerant fiber sensor based on BOTDR system," *Optoelectron. Lett.*, Vol. 18, No. 6, pp. 343-348, 2022. <https://doi.org/10.1007/s11801-022-1172-0>
- [15] A. Zafeiropoulou et al., "D-shaped multicore fibre for distributed curvature sensing with BOTDR," *Optical Sensors and Sensing Congress, OSA Technical Digest*, No. STh3G.1, 2020. <https://doi.org/10.1364/SENSORS.2020.STh3G.1>
- [16] W. Zou et al., "Experimental study of Brillouin scattering in fluorine doped single-mode optical fibers," *Opt. Express*, Vol. 16, pp. 18804-18812, 2008. <https://doi.org/10.1364/OE.16.018804>
- [17] M. Łakomski, M. Plona, B. Guzowski, I. S. M. Shatarat, "The impact of Optical Fiber Type on the Temperature Measurements in Distributed Optical Fiber Sensor Systems," *Pomiary Automatyka Robotyka*, Vol. 27, No. 3/2023, pp. 27-32, 2023. https://doi.org/10.143113/PAR_249/27